Received: 25 January 2019 | Revised: 24 May 2019 | Accepted: 11 June 2019

DOI: 10.1002/jbm.b.34438

ORIGINAL RESEARCH REPORT

Society For Biomaterials WILEY

Use of tendon to produce decellularized sheets of mineralized collagen fibrils for bone tissue repair and regeneration

Brendan H. Grue[1] | Samuel P. Veres[1,2]

[1]Division of Engineering, Saint Mary's University, Halifax, Nova Scotia

[2]School of Biomedical Engineering, Dalhousie University, Halifax, Nova Scotia

Correspondence
Samuel P. Veres, Division of Engineering, Saint Mary's University, 923 Robie Street, Halifax, NS B3H 3C3.
Email: sam.veres@smu.ca

Funding information
Nova Scotia Health Research Foundation; Natural Sciences and Engineering Research Council of Canada, Grant/Award Number: RGPIN-2014-04967

Abstract

With demand for alternatives to autograft and allograft materials continuing to rise, development of new scaffolds for bone tissue repair and regeneration remains of significant interest. Engineered collagen-calcium phosphate (CaP) constructs can offer desirable attributes, including absence of foreign body response and possession of inherent osteogenic potential. Despite their promise, current collagen-CaP constructs are limited to nonload-bearing applications. In this article, we describe a process for creating decellularized sheets of highly aligned, natively cross-linked, and mineralized collagen fibrils, which may be useful for developing multilaminate collagen-CaP constructs with improved mechanical properties. Decellularized bovine tendons were cryosectioned to produce thin sheets of aligned collagen fibrils. Mineralization of the sheets was then performed using an alternate soaking method incorporating a polymer-induced liquid precursor (PILP) process to promote intrafibrillar mineralization, along with incorporation of physiologically relevant amounts of citrate, Mg, and carbonate. Characteristics of the produced scaffolds were assessed using energy-dispersive X-ray spectroscopy (EDX), scanning electron microscopy (SEM), and transmission electron microscopy (TEM). Scaffolds were also compared with both native bovine cortical bone and pure hydroxyapatite using X-ray powder diffraction (XRD), and Fourier transform infrared spectroscopy attenuated total reflection (FTIR-ATR). Structural and chemical analyses show that the scaffold preparation process that we described is successful in creating mineralized collagen sheets, possessing a mineral phase similar to that found in bone as well as a close association between collagen fibrils and mineral plates.

KEYWORDS

bone scaffold, chemical and nanostructural analysis, collagen mineralization, engineered graft, tissue repair and regeneration

1 | INTRODUCTION

Critical size defects in bone are those sufficiently large to prevent spontaneous healing and can occur due to injury, illness, or through surgical procedures, such as osteotomy (Schemitsch, 2017), (Schmitz & Hollinger, 1986). Defects that are large enough to require surgical intervention are typically filled using autologous bone tissue, usually taken from the iliac crest (Wasiak, 2015). While success rates using autologous grafts are high, limited graft availability and donor site morbidity remain serious concerns. To overcome these limitations, alternatives including allografts, xenografts, and engineered materials have been used. Other issues, however, exist for the currently available alternatives, including immunogenicity, undesirable degradation rates or by-products, and unfavorable mechanical characteristics.

As an alternative to synthetic void filler materials, such as polylactic acid, polyglycolic acid, polyurethanes, and others (Marzec, Kucińska-Lipka, Kalaszczyńska, & Janik, 2017), interest in engineered mineralized collagen composite scaffolds is increasing. Commonly used methods for preparing mineralized collagen scaffolds include formation of matrix from soluble collagen followed by exposure to a mineral containing solution for several hours (Wang et al., 2018), or coprecipitation of mineral and collagen mixtures (Tomoaia & Pasca, 2015). Mineralized collagen scaffolds may be ideal materials for bone defect repair due to their chemical, structural, and mechanical similarity to native bone. In a study conducted by Lyons et al. (2014), a collagen-hydroxyapatite (HA) scaffold exhibited comparable healing to autologous bone grafts in a rabbit radius osteotomy defect model. These scaffolds were prepared through the dissolution of collagen in an acidic solution followed by freeze-drying a mixture of mineral and collagen (Lyons et al., 2014). Pugely et al. (2017) investigated two bone void fillers composed of HA, tricalcium phosphate (TCP), and bovine collagen, with one also containing Bi-Ostetic bioactive glass foam. Both fillers exhibited biocompatibility and efficacy in bone healing using an established rabbit posterolateral fusion model (Pugely et al., 2017). In a study conducted by Zheng et al. (2014), a β-TCP/collagen composite filler (Cerasorb® Orhto Foam) was tested in a rabbit distal femoral condyle model and resulted in complete resorption and bone formation without toxic or immunologic effects. A bilayered biomimetic scaffold composed of an inner type I collagen layer and an outer layer of mineralized collagen (30%) and Mg doped HA (70%) was evaluated by Calabrese et al. (2016) through subcutaneous implantation in mice. This bilayered scaffold was able to recruit host cells and produce new mineral formation by the host tissue throughout its ectopic location as well as neovascularization (Calabrese et al., 2016). Weisgerber et al. (2015) prepared mineralized collagen-glycosaminoglycan (GAG) scaffolds through the lyophilization of a collagen-calcium salt suspension in custom molds. These scaffolds were then cross-linked in a solution of 1-ethyl-3-(3-dimethylaminopropyl)-carbodiimide (EDC) and N-hydroxysuccinimide (NHS) before culturing with human mesenchymal stem cells (MSCs), where they exhibited enhanced osteogenesis compared with nonmineralized controls (Weisgerber et al., 2015). In a study by Lin et al. (2016), composite type I collagen-HA scaffolds were produced through low-temperature additive manufacturing. Through in vitro investigations, these scaffolds showed enhanced bone marrow stromal cell proliferation compared to nonprinted scaffolds (molded) and were remodeled successfully when used in a rabbit femoral condyle defect model (Lin et al., 2016). Additionally, Wang et al. (2018) constructed a mineralized collagen scaffold through the immersion of type I collagen in a mineral containing solution for 48 hr. The scaffold was found to promote MSC adhesion, proliferation, and osteogenic differentiation in vitro as well as ectopic bone formation and enhanced bone growth in a skull-penetrating SD rat defect model when compared with blank control and collagen membrane groups at both 4 and 12 week timepoints (Wang et al., 2018).

While the engineered mineralized collagen scaffolds mentioned above have shown promise in their ability to aid tissue regeneration, further benefits and new surgical applications may be realized by developing scaffolds that: (a) possess mineral that more closely mimics that present in native bone, and (b) offer improved structural control of the organic collagen phase.

Achieving the correct mineral structure when creating mineralized collagen scaffolds may be biologically important. The mineral phase found within native bone tissue has a nonstoichiometric, poorly crystalline apatite structure, close to that of HA, $Ca_5(PO_4)_3(OH)$ (Olszta et al., 2007). The poorly crystalline nature of the mineral phase is partly due to the incorporation of various chemical and ionic species within the apatitic mineral, including carbonate (4–6%), Na (0.9%), and Mg (0.5%) (Olszta et al., 2007). Bone graft substitutes have largely focused on the use of CaP materials, such as HA, to induce device integration at the defect site. Incorporation of cationic or anionic additives into these CaP-based mineral preparations has received much less study. These minor constituents may act to enhance recognition and remodeling of the implanted materials via their interactions with native osteogenic cells. For instance, Mg^{2+} may play an important role in the production of nitric oxide, which aids in the modulation of angiogenesis (Zhang, Wu, Chen, & Lin, 2018). Mg^{2+} may also help stimulate osteoblast proliferation (Landi et al., 2008). When added to HA, carbonate was found to enhance osteoconductivity and bioresorption of mineral (Zhang et al., 2018).

Current mineralized collagen fillers are typically produced from aqueous collagen suspensions or slurries that are precipitated or molded into shape (Gelinsky et al., 2008; Girija et al., 2004; Goes et al., 2007; Kikuchi et al., 2001; Liao et al., 2005; Lickorish et al., 2004; Liu et al., 2011; Tampieri et al., 2003; Villa et al., 2015; Yokoyama et al., 2005). The resulting fillers are composed of randomly oriented collagen fibrils, which may additionally lack native enzymatic cross-linking if produced from suspensions of collagen monomers. Because the mechanics of collagen materials depend highly on collagen fibril alignment, improved control of collagen fibril alignment in mineralized fillers would be highly advantageous. In terms of maintaining native intermolecular cross-linking within fibrils, this may have biological in addition to mechanical importance. While intermolecular cross-linking is required to both limit the rate of scaffold degradation and improve mechanical stability, various forms of exogenous cross-linking have been shown to promote a proinflammatory response (Delgado et al., 2015), suggesting that incorporation of native lysyl oxidase (LOX)-mediated cross-linking may be important for optimization of a scaffold's regenerative potential. LOX cross-linking may also influence osteoblast and osteoclast differentiation (Ida et al., 2018), providing an additional means to influence osteogenesis.

Biomimetic mineralization of well-structured collagen fibrils presents various challenges, however. First, in isolation from other matrix components, collagen fibrils may lack the molecular functionality required to induce both intrafibrillar and extrafibrillar mineralization. For example, various acidic noncollagenous proteins rich in aspartic and glutamic acid residues are found throughout the bone tissue

microenvironment and are thought to play a role in intrafibrillar mineralization of collagen fibrils. The action of these proteins was simulated by Gower and Odom (2000) where only after the addition of polyaspartic acid (pAsp) to the mineral containing solutions was intrafibrillar mineralization achieved. It was thought that these process directing polymers caused the mineral phase to form a polymer-induced liquid-phase precursor (PILP), which was able to penetrate the small gap regions in the collagen fibrils before further nucleation, forming mineralized collagen fibrils better resembling those found within native bone tissue (Gower, 2008; Olszta et al., 2003). Second, the exact chemical structure and geometry of the poorly crystalline, carbonated HA found within bone has proved difficult to reproduce ex vivo (Olszta et al., 2007; Zhang et al., 2018). For intrafibrillar mineral integration and deposition to occur, the geometry in which the incoming mineral phase exists must be carefully regulated. If the incoming mineral phase can nucleate and crystallize into relatively large crystals, size constraints will inhibit occupancy within collagen fibrils (Gower, 2008). Modifications to crystal size and composition may affect how well a scaffold integrates with bone as well as degradation rate and by-products.

In this study, we describe a process for preparing mineralized collagen sheets, with organic phase composed of highly aligned, natively structured collagen fibrils, and mineral phase sharing chemical similarities to that found in native bone. In characterizing the resulting scaffold structures, the effects of pAsp and citrate additions during the mineralization process are explored. Evaluations of scaffold mineralization and surface architecture were made through use of scanning electron microscopy (SEM) and transmission electron microscopy (TEM). Mineral phase identification and characterization were performed using energy-dispersive X-ray spectroscopy (EDX), X-ray powder diffraction (XRD), and Fourier transform infrared spectroscopy attenuated total reflection (FTIR-ATR). The process that we describe for producing single, mineralized collagen sheets may be useful for creating larger, load-bearing, regenerative orthopaedic devices.

2 | MATERIALS AND METHODS

2.1 | Tendon acquisition and decellularization

Common digital extensor (CDE) tendons were dissected from the forelimbs of steers aged 24–36 months, killed for food at a local abattoir. Dissected tendons were stored in phosphate-buffered saline (PBS) solution at 4°C to await decellularization treatment, which was started within 12 hr of dissection.

Decellularization treatment was conducted following a method previously described by Woods and Gratzer (2005). Briefly, tendons were first exposed to a hypotonic 10 mM tris buffer, containing serine and metalloprotease inhibitors, along with 1% penicillin/streptomycin and 1% amphotericin B for 36 hr at room temperature. Tendons were then moved to a high saline 50 mM tris buffer containing 1% Triton X-100 along with antibiotics and protease inhibitors for 48 hr at room temperature, followed by Hanks' buffer rinse and wash in a DNase/RNase solution. This was followed by a 48 hr, room temperature soak in 1% Triton X-100 solution with 50 mM TRIZMA® base and antibiotics. Finally, the tendon samples were rinsed in PBS with antibiotics and stored in a similar solution at 4°C until further use.

2.2 | Cryosectioning and phosphorylation

Decellularized tendons were cryosectioned using a Leica SM2000R sliding microtome. Tendons were cut into 2-cm-long segments, mounted on a steel block using optimal cutting temperature (OCT) compound, frozen in liquid nitrogen, and sectioned longitudinally to produce 200-μm-thick collagen sheets. The collagen sheets were then phosphorylated via treatment with STMP to enhance mineralization (Gu et al., 2010; Li & Chang, 2008). A solution of 2.5 wt % sodium trimetaphosphate (STMP) was hydrolyzed at pH 12 for 5 hr (Shen, 1966). The solution was then adjusted to pH 10. Collagen sheets were treated in STMP solution for 1 hr at room temperature under constant agitation. The sheets were then rinsed in ddH_2O before beginning the alternate soaking mineralization procedure.

2.3 | Mineralization

Mineralization of the phosphorylated collagen sheets was performed using a modified form of the alternate soaking process described by Taguchi et al., (1999). Using a stainless-steel mesh basket, sheets were first soaked in 200 mL ddH_2O before soaking in 200 mL of a magnesium doped (0.01 M) calcium solution ($CaCl_2/MgCl_2$, 200 mM) within a temperature-controlled water bath at 37°C for 120 s at pH 7.4. The sheets were then briefly rinsed in ddH_2O before soaking for an additional 120 s in a 120 mM sodium phosphate solution containing 0.025 M sodium carbonate at 37°C and pH 7.4. The progression of collagen sheets through these four solutions constituted a single mineralizing cycle (Figure 1). For this study, sheets underwent 10 mineralization cycles.

2.4 | pAsp and citrate additions to the mineralization process

To promote intrafibrillar mineralization, pAsp (mean molecular weight (MW) 29 kDa, Alamanda Polymers, Huntsville, AL) was added to the alternate soaking process during the mineralization of some of the collagen sheets. For the mineralization of those sheets, the calcium and phosphorous solutions each contained 100 μg/mL of pAsp. To better match the chemical environment of natural bone tissue, citrate (Sigma-Aldrich, Oakville, ON) was also added to the alternate soaking process during the mineralization of some collagen sheets. Citrate was only added to the calcium solution at a concentration of 0.02 M.

2.5 | Sample groups

With the addition of pAsp and citrate to the mineralization process, the study included four sample groups:

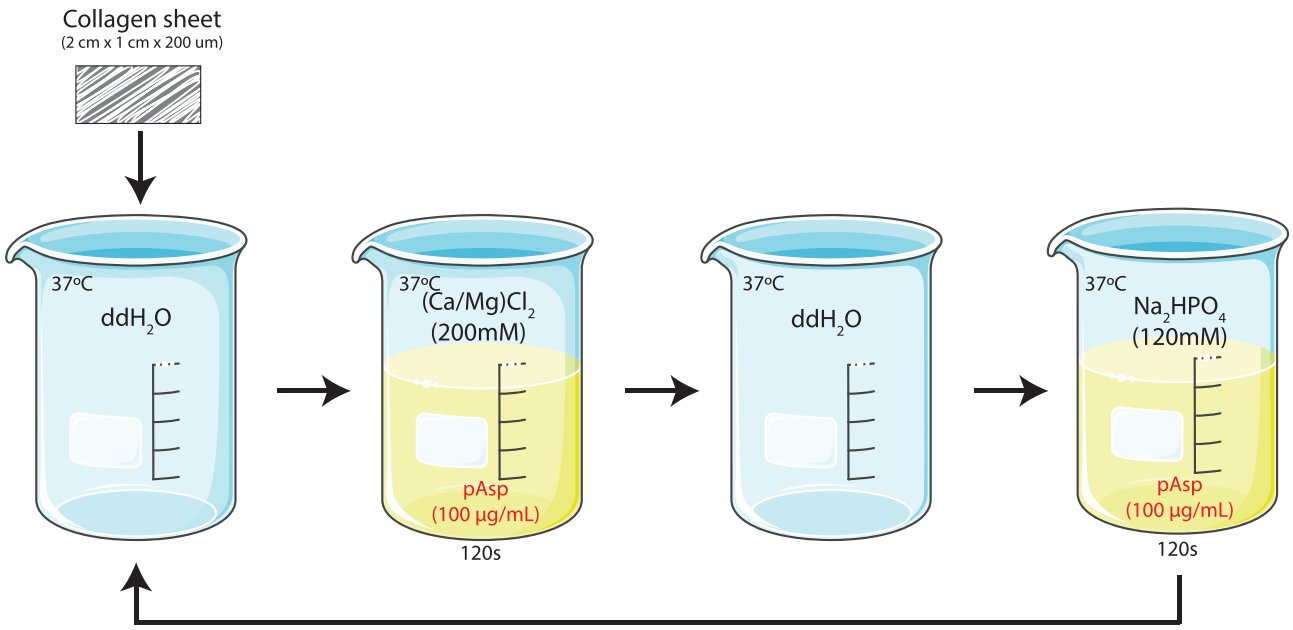

FIGURE 1 Schematic of the alternate soaking process used to mineralize sheets of highly aligned, natively structured collagen fibrils derived from decellularized bovine tendon

- Mineralized +pAsp / +citrate group: these scaffolds were mineralized with additions of both pAsp and citrate to treatment process.
- Mineralized +pAsp / −citrate group: these scaffolds were mineralized with addition of pAsp, but without citrate addition.
- Mineralized −pAsp / +citrate group: these scaffolds were mineralized with addition of citrate, but without pAsp.
- Unmineralized group: these scaffolds consisted of cryosectioned sheets of decellularized tendon that were phosphorylated, but did not undergo subsequent mineralization.

2.6 | Scanning electron microscopy (SEM) and energy-dispersive X-ray spectroscopy (EDX)

Ultrastructural and elemental analyses of both mineralized and unmineralized collagen sheets were performed using a SEM (model S-4700, Hitachi, Tokyo, Japan) and integrated EDX with precision approaching 0.1% (model X-Max, Oxford Instruments, Abingdon, United Kingdom). The collagen sheets were prepared for analysis by fixation in 2.5% electron microscopy-grade glutaraldehyde in PBS for 1 hr at room temperature under constant agitation, followed by rinsing in ddH_2O, and dehydration in graded ethanol. Sheets were then critical point dried, mounted on SEM stubs using carbon tape, and coated with gold-palladium. The coated samples were viewed under SEM at 3–5 kV, 10–15 µA. To better visualize the relationship between collagen fibrils and the introduced mineral phase, some scaffolds were etched prior to glutaraldehyde fixation using 0.1 M HCl under constant agitation for 2 min before rinsing in ddH_2O. For each of the four sample groups, three scaffolds prepared from the CDE tendons of different animals and mineralized in different treatment batches were examined using SEM. Only the mineralized +pAsp / +citrate scaffolds were assessed via EDX, which was conducted at 10 kV. For the three mineralized +pAsp / +citrate scaffolds assessed under SEM, EDX measurements were taken at a total of eight locations, the results of which were then averaged.

2.7 | Transmission electron microscopy (TEM)

Mineralized and unmineralized sheets were also assessed using a FEI Tecnai 12 TEM (Thermo Fisher Scientific, Waltham, MA). Samples were pulverized in liquid nitrogen, dispersed in ethanol, collected on copper TEM grids, and examined unstained at 120 kV. For each of the three mineralized sample groups, samples from three scaffolds prepared from the CDE tendons of different animals and mineralized in different treatment batches were examined using TEM. A sample from an unmineralized scaffold was also examined.

2.8 | X-ray powder diffraction (XRD) and Fourier transform infrared spectroscopy attenuated total reflection (FTIR-ATR)

Mineralized +pAsp / +citrate scaffolds were assessed using XRD and FTIR-ATR and compared with samples of bovine cortical bone and pure HA. Cortical bone samples were prepared from the mid-diaphysis of metacarpals 3 and 4 from the collected bovine forelimbs. Samples 2-cm-long were cut, boiled in ddH_2O for 30 min, dried at 100°C for 22 hr, processed into a coarse powder using a hacksaw, and then fine powder using a mortar and pestle. A mortar and pestle was similarly used to produce fine powders from the pure HA and prepared mineralized scaffolds. XRD was conducted using Cu-Kα X-ray radiation from a Siemens D500 Diffractometer at 30 kV and 30 mA, using a step size of

0.05° over a 2θ range of 20°–50°. XRD peaks were recognized by referring to JCPDS file number 00-009-0432 (hydroxylapatite, syn). FTIR-ATR was conducted using a Bruker Alpha Platinum-ATR FTIR spectrometer in the 400–4000 cm^{-1} range averaged over 24 scans per sample with a resolution of 4 cm^{-1}. For each of the three mineralized sample groups, samples from three scaffolds prepared from the CDE tendons of different animals and mineralized in different treatment batches were assessed using XRD and FTIR-ATR.

3 | RESULTS

All numerical data are presented as mean ± *SD*.

3.1 | Scaffold ultrastructure

SEM and TEM were performed on collagen sheets mineralized with additions of both pAsp and citrate (mineralized +pAsp / +citrate group), without citrate (mineralized +pAsp / –citrate group), and without pAsp (mineralized –pAsp / +citrate group). Unmineralized collagen sheets were also assessed.

SEM examination of unmineralized collagen sheets showed that the highly aligned fibril arrangement typical of tendon was preserved during decellularization treatment and cryosectioning (Figure 2a,b). SEM examination of the mineralized +pAsp / +citrate sheets showed that the introduced mineral phase formed plate-like crystals covering the fibrils, with accumulation of extrafibrillar spherulites (Figure 2c,d). Similarly prepared sheets etched prior to preparation for SEM using dilute HCl to better visualize the underlying mineral-collagen interface showed mineral bridging between adjacent collagen fibrils (Figure 3a,b). When samples from the mineralized +pAsp / + citrate scaffolds were viewed unstained under TEM, individual mineralized collagen fibrils were observed with plate-like crystals longitudinally aligned with the fibrils (Figure 4a,b). Unlike the fibrils from scaffolds mineralized without pAsp or citrate, described below, D-banding could not be seen on these fibrils under TEM, possibly due to the abundance of mineral present.

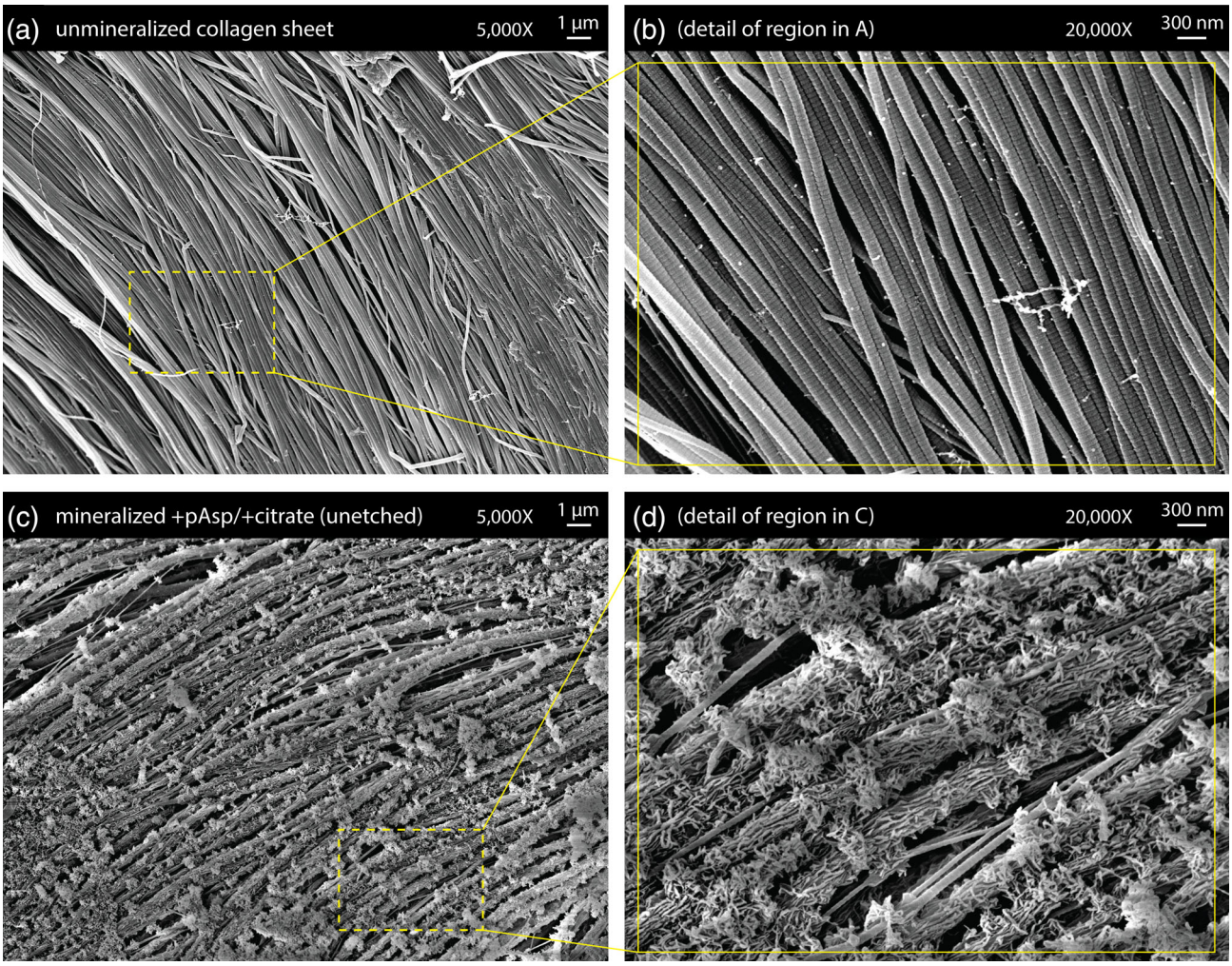

FIGURE 2 (a,b) Low and high magnification scanning electron microscopy (SEM) images of a decellularized sheet of collagen fibrils from bovine tendon prior to mineralization. (c,d) Low and high magnification SEM images of a similar collagen sheet after mineralization via 10 cycles of alternate soaking with both pAsp and citrate additives. Individual collagen fibrils are covered in plate-like crystals, with larger spherical clusters of mineral frequently occurring. Unlike the sheets shown in Figure 3, the sheets shown here are unetched

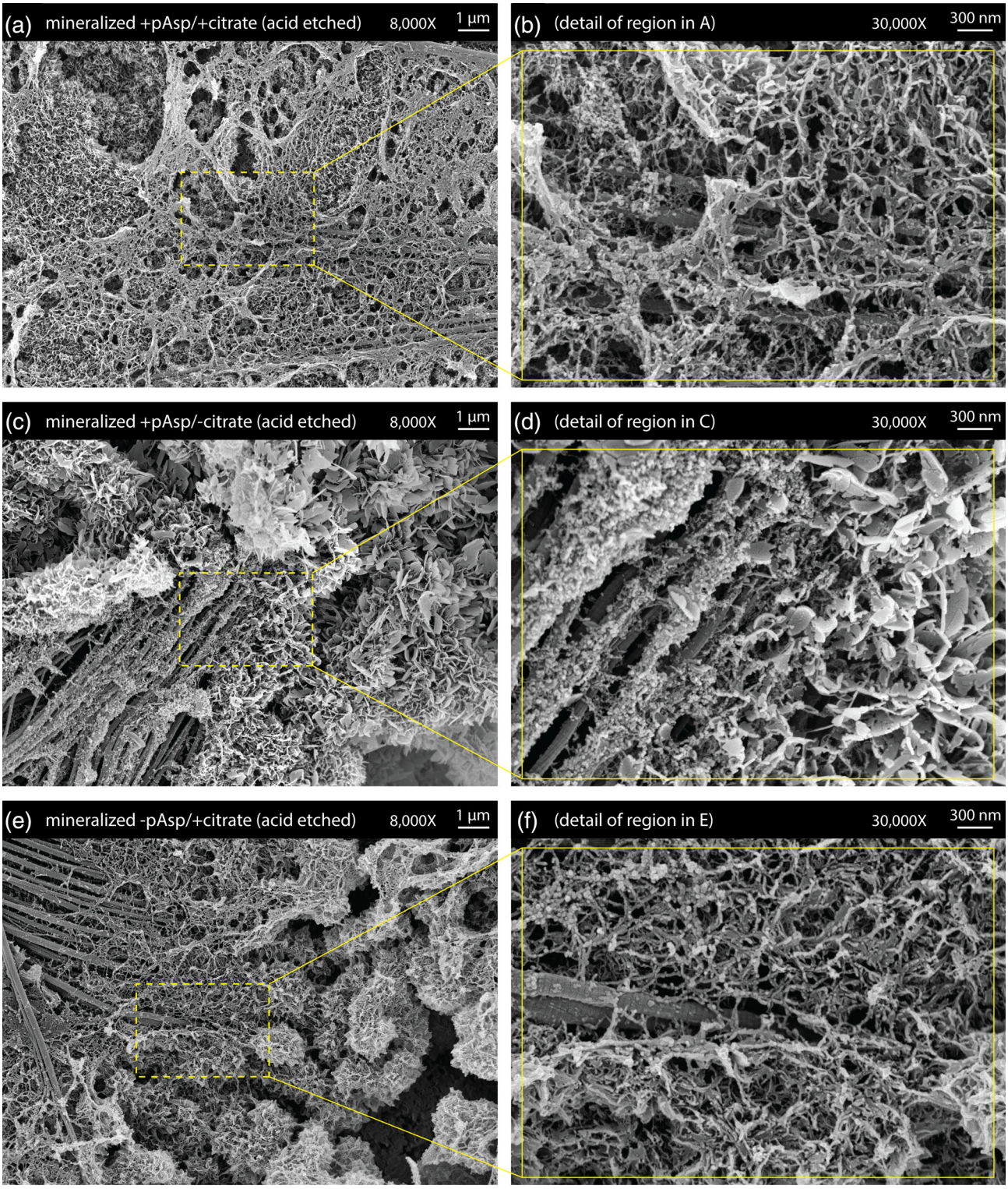

FIGURE 3 Scanning electron microscopy (SEM) images of acid-etched mineralized collagen sheets. (a,b) Sheets prepared with pAsp and citrate additions to the mineralization treatment process showed mineral bridging between collagen fibrils. (c,d) Absence of citrate from the mineralization process led to extrafibrillar plate-like crystals growing much larger in size. (e,f) Absence of pAsp from the mineralization process led to excessive accumulation of extrafibrillar spherulites

For samples prepared with the absence of citrate only (mineralized +pAsp / −citrate scaffolds), SEM after acid-etching revealed the presence of much larger plate-like crystals than were observed when citrate was present (Figure 3c,d vs. 3a,b). TEM similarly showed that these samples contained larger plate-like crystals when compared with the mineralization treatments that included citrate (Figure 4c,d vs. 4a,b).

Acid-etched sheets that were prepared in the absence of only the process directing agent, pAsp, (mineralized −pAsp / +citrate scaffolds)

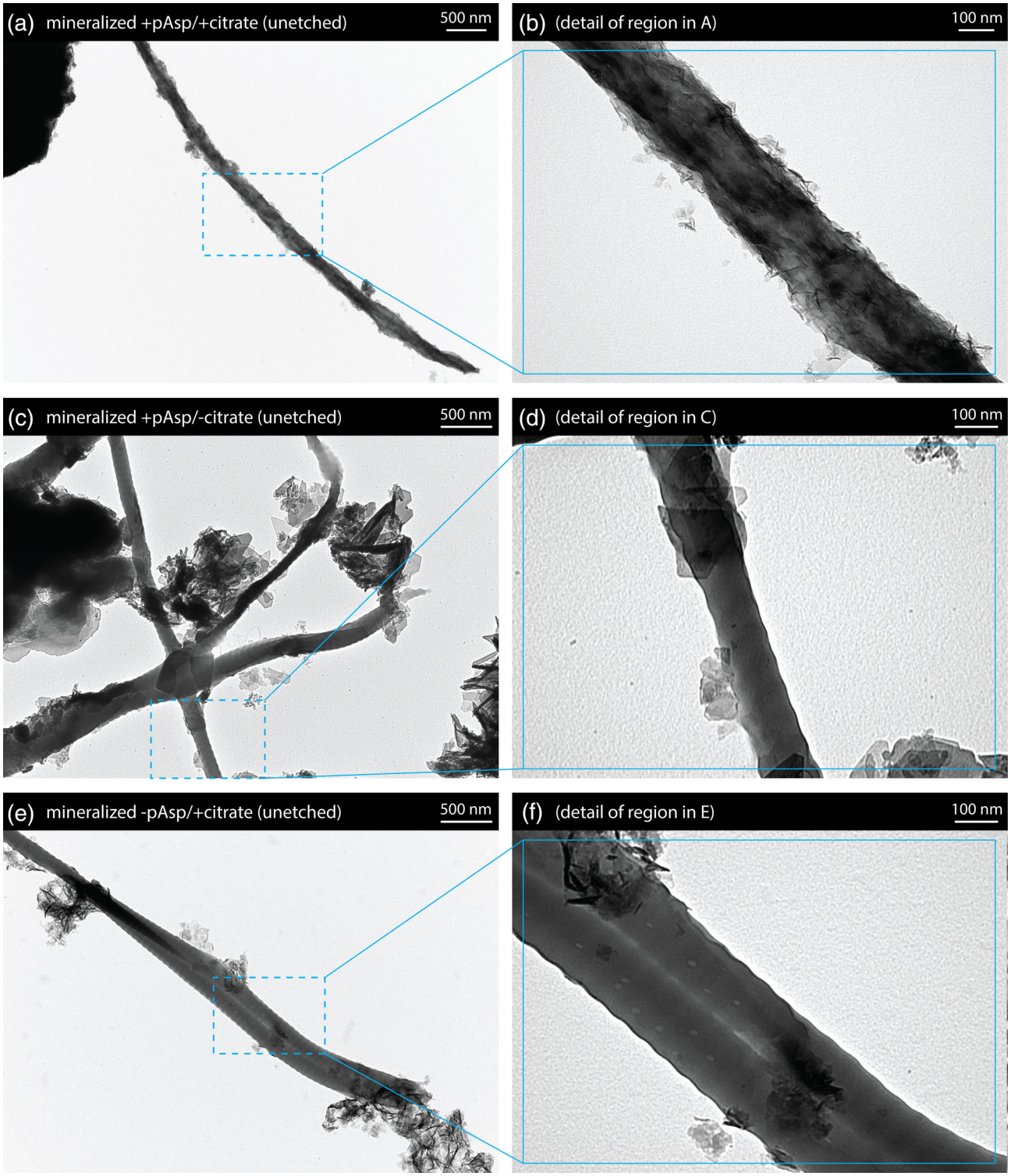

FIGURE 4 Transmission electron microscopy (TEM) images of collagen fibrils removed from the unetched mineralized collagen sheets. (a,b) Sheets mineralized with pAsp and citrate additions contained collagen fibrils incorporating a high density of small, longitudinally aligned crystals. D-banding was not apparent, presumably due to the quantity of mineral present. (c,d) For sheets mineralized without citrate, much larger plate-like crystals were seen. (e,f) Sheets prepared without addition of the PILP process directing agent pAsp contained fibrils with a reduced quantity of closely associated mineral

were found to contain greater amounts of extrafibrillar spherulites when observed under SEM (Figure 3e,f). In TEM, it was evident that the absence of pAsp greatly reduced the amount of mineral associated with the collagen fibrils. Compared with fibrils from the mineralized +pAsp / +citrate scaffolds (Figure 4a,b), those from the scaffolds prepared without pAsp possessed noticeably fewer plate-like crystals (Figure 4e,f).

3.2 | Mineral phase analysis

3.2.1 | Energy-dispersive X-ray spectroscopy (EDX)

Elemental compositions for three mineralized +pAsp / +citrate scaffolds were assessed by EDX. Mean weight percent (wt %) for O, C, Ca, P, Na, and Mg within the mineral phase of the sheets was 47.13, 12.42, 26.23, 13.90, 0.25, and 0.08 wt %, respectively (Figure 5), yielding a Ca/P ratio of 1.89.

3.2.2 | X-ray powder diffraction (XRD)

XRD was performed on the mineralized +pAsp / +citrate scaffolds, cortical bone powder, and pure HA. XRD patterns for the mineralized +pAsp / +citrate scaffolds were similar to those of native cortical bone, with peak positions similar to pure HA but significantly broadened (Figure 6), indicating small crystallite size and presence of chemical substitutions. Both cortical bone and mineralized scaffolds contained the (002) peak found at approximately 26° for pure HA, and the (211), (112), and (300) peaks for pure HA appeared as a single broadened peak in both bone and mineralized scaffolds. Compared with cortical bone, peaks for the mineralized scaffolds were somewhat weaker and broader. While both bone and pure HA contained smaller peaks near 40°, 47°, and 50°, these were not observed for the mineralized scaffolds.

3.2.3 | Fourier transform infrared spectroscopy attenuated total reflection (FTIR-ATR)

Absorption bands for the mineralized +pAsp / +citrate scaffolds, cortical bone, and pure HA were obtained through FTIR-ATR. The characteristic banding of the PO_4^{3-} groups was visible in all three samples (Figure 7), with the asymmetric O-P-O bending modes occurring at approximately 560 cm^{-1} and the asymmetric P-O stretching mode visible at approximately 1,020 cm^{-1} (Berzina-Cimdina & Borodajenko, 2012; Ulian et al., 2013). As expected, weak intensity bands between 3100 and 3500 cm^{-1} attributed to the N-H of the amide of collagen were observed for both cortical bone and mineralized scaffolds. Doublet peaks at around 1450 and 1640 cm^{-1} and a peak at 873 cm^{-1} were also present, attributable to the vibrational frequencies of carbonate ions substituted into apatite at the phosphate and OH^- sites (Farzadi et al., 2014; Meejoo et al., 2006). The band at approximately 1650 cm^{-1} on both cortical bone and mineralized scaffold spectra is most likely attributable to OH^-, carbonate ions, H_2O, or a combination of the former with contribution from the amide I band of collagen (Berzina-Cimdina & Borodajenko, 2012; Manjubala & Sivakumar, 2001; Raynaud et al., 2002; Talari et al., 2017).

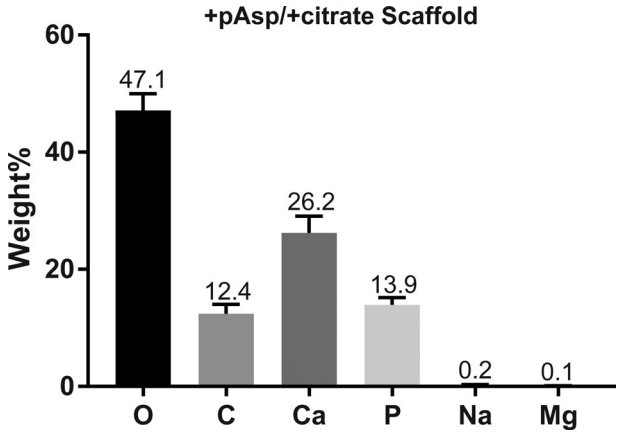

FIGURE 5 Energy-dispersive X-ray spectroscopy (EDX)-derived elemental composition of collagen sheets mineralized with pAsp and citrate additions showed a Ca/P wt % ratio of approximately 1.89, similar to native bone, with small quantities of Mg and Na present within the prepared mineral phase

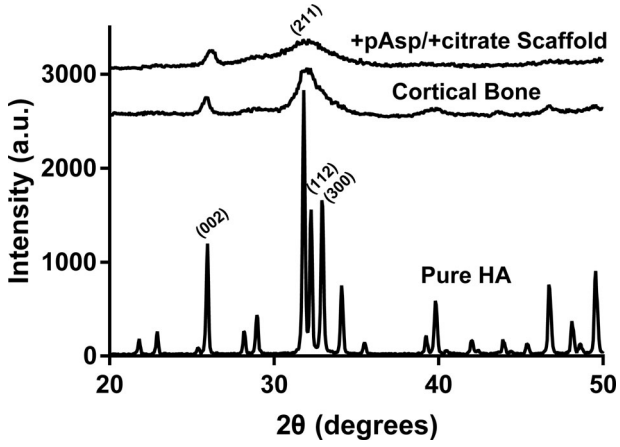

FIGURE 6 X-ray powder diffraction (XRD) peaks of collagen sheets mineralized with pAsp and citrate additions, compared with those from native bovine cortical bone and pure hydroxyapatite (HA)

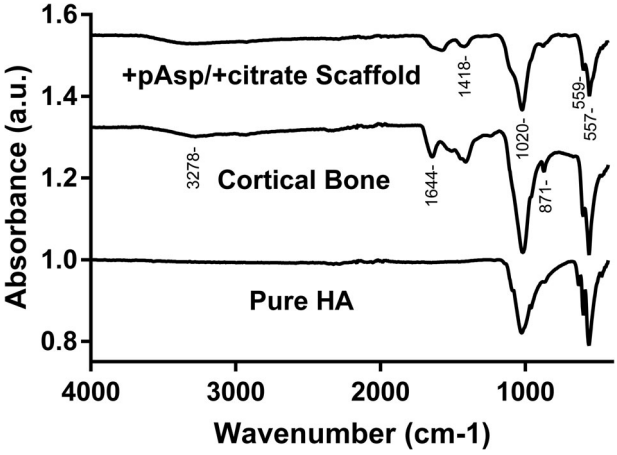

FIGURE 7 Fourier transform infrared spectroscopy attenuated total reflection (FTIR-ATR) spectra of collagen sheets mineralized with pAsp and citrate additions, compared with those from native bovine cortical bone and pure hydroxyapatite (HA)

4 | DISCUSSION

Many of the previous approaches to creating mineralized collagen scaffolds for bone tissue repair and regeneration have relied on the use of reconstituted collagen, with the mineral phase either incorporated into the scaffold during tropocollagen aggregation (Gelinsky et al., 2008; Kikuchi et al., 2001; Liao et al., 2005; Tampieri et al., 2003; Villa et al., 2015; Yokoyama et al., 2005) or following assembly of a collagen template (Girija et al., 2004; Goes et al., 2007; Lickorish et al., 2004; Liu et al., 2011). Although desirable from an ease-of-manufacturing standpoint, approaches based on reconstituted collagen monomer assembly have not been able to recreate scaffolds of well-aligned, natively cross-linked collagen fibrils, potentially limiting their functionality. In this article, we have taken a different approach, using cryosectioned sheets of decellularized bovine tendon to provide an acellular template of highly aligned, well-cross-linked collagen fibrils into which carbonated HA has subsequently been incorporated. By combining sheets of densely packed, uniaxially aligned collagen fibrils to form a multilaminate construct, it may be possible to produce a scaffold with the regenerative potential inherent to mineralized collagen (Lyons et al., 2014), and load-bearing capacity required to effectively support the defect site.

Early crystal nucleation on the surface of collagen fibrils in vivo is thought to be inhibited by various ionic or macromolecular constituents, allowing amorphous mineral phases to penetrate the gap regions of collagen fibrils, resulting in intrafibrillar mineralization (Gower & Odom, 2000). Nonclassical crystallization pathways may allow for kinetically rather than thermodynamically driven crystal formation mechanisms, leading to development of the complex crystal structures found in bone and elsewhere in nature (Cölfen, 2007). Kinetically driven crystal formation is usually supported through the presence of polyelectrolytes, or other soluble macromolecules or ions that affect the surface energy of forming crystals at specific faces or, as is thought to be the case for bone, may initially prevent crystal formation altogether by creating a liquid precursor (Cölfen, 2007). In the current study, mineralization treatment of the collagen sheets without addition of pAsp led to the development of extrafibrillar spherulitic clusters (Figure 3e,f), consistent with the work of others (Jee et al., 2010; Gower, 2015). When mineralization was conducted with pAsp, fewer extrafibrillar spherulites were formed and an increase in plate-like crystals intimately associated with individual collagen fibrils was observed (Figures 2d and 4b). These observations are consistent with previous experiments where reduction in crystal size and increase in intrafibrillar mineralization were thought to be promoted by the addition of pAsp to the mineralization solutions through a crystal nucleation-limiting mechanism (Gower, 2008; Kim et al., 2018; Nudelman et al., 2010).

Along with pAsp, it is likely that citrate and inorganic ions, such as Mg^{2+} and PO_4^{3-}, contributed to the crystal structures seen in the current study. It has been proposed that citrate penetrates collagen fibrils where it then provides additional nucleation sites for intrafibrillar calcium-phosphate crystal growth (Shao et al., 2018). Additionally, when adsorbed on collagen fibrils, citrate has been reported to improve wetting between collagen and the mineral precursor phase (Shao et al., 2018). These effects appear to promote intrafibrillar mineralization, even in the absence of pAsp (Delgado-López et al., 2017). It has also been reported that the presence of citrate during mineralization contributes to a reduction in extrafibrillar mineral plate-size (Hu et al., 2010; Iafisco et al., 2015; Xie & Nancollas, 2010). This was indeed observed in the current study, where mineralization solutions containing pAsp but lacking citrate lead to the formation of large extrafibrillar mineral plates (Figure 4d vs. b). Use of citrate during collagen mineralization for scaffold production may be important for increasing intrafibrillar mineralization, increasing scaffold homogeneity, and increasing potential sites for cellular interaction through reduction in extrafibrillar mineral plate size. As with other additives to the mineralization solutions, further investigations, however, toward the extent and complete characteristic profile of citrate incorporation within the mineral phase structure may be warranted, along with a complete analysis of its effects on scaffold functionality, to support its use in the manufacture of future bone repair devices.

In addition to pAsp and citrate incorporation into the mineralization process, the present study also used phosphorylation via STMP treatment, and Mg and carbonate additives. Unlike pAsp and citrate, these were used in the preparation of all mineralized scaffolds produced, and no attempt was made to assess their individual contributions to the mineralized structures produced. STMP has a long history for phosphorylation of proteins in the food industry (Li et al., 2010; Matheis & Whitaker, 1984), and phosphorylation of collagen using STMP has previously been described in detail (Gu et al., 2010; Li & Chang, 2008; Shen, 1966). Under alkaline conditions, STMP is hydrolyzed to produce sodium tripolyphosphate, which is believed to phosphorylate serine, threonine, and tyrosine residues through covalent bonding with side-chain oxygen (Gu et al., 2010). That STMP is effective in aiding collagen mineralization, likely via the ability of phosphate groups to attract amorphous calcium phosphate precursors, is supported by prior studies of in vitro mineralization of dentin and dermal collagen (Gu et al., 2010; Li et al., 2010). Meanwhile, the presence of Mg^{2+} during mineralization has been shown to improve the stability of PILP and amorphous mineral phases (Cheng et al., 2007; Politi et al., 2009), and allow wetting of protein matrices by PILP (Berg et al., 2013), while incorporation of carbonate during synthetic apatite formation has been shown to result in crystal structures with high similarity to those present in native bone (Chatelain et al., 2013; Liao et al., 2005; Linhart et al., 2001; Moradian-Oldak et al., 1991).

To examine the atomic composition and crystallographic structure of the mineral phase within the prepared collagen sheets, EDX, XRD, and FTIR-ATR were used. EDX analysis of the scaffolds indicated a Ca/P molar ratio of 1.46, close to known Ca/P molar ratios for various forms of calcium phosphates: 1.33 for octacalcium phosphate, 1.5 for amorphous calcium phosphate and calcium deficient HA, 1.67 for precipitated HA, 1.8 for Na and carbonate containing apatite and 2.0 for heavily carbonated HA (Driessens et al., 1994). For human bone, Ca/P molar ratios typically range from 1.19 to 2.28 (Fountos et al., 1999; Mousa & Hanna, 2013; Tzaphlidou & Zaichick, 2004).

As summarized by Driessens and Verbeeck (1990), the atomic fractions by weight percentage of O, C, Ca, P, Na, and Mg in bone are 43.5, 15.5, 22.5, 10.3, 0.1, and 0.2, respectively, similar to the mineral phase composition of the scaffolds that were produced in the current work (Figure 5). XRD comparisons between the prepared sheets and bovine cortical bone indicated similar broad profiles with conserved HA-like peaks at around 26° (002) and 32° (211, 112, 300) indicating that both mineral phases consisted of poorly crystalline or amorphous HA. XRD profiles for the mineralized collagen sheets were somewhat duller and possessed broader peaks, perhaps indicating a more amorphous mineral composition compared with that of the 2 to 3-year-old bovine cortical bone (Figure 6). Greater content of amorphous mineral would be representative of that found earlier in bone tissue development (Posner & Betts, 1975; Rey et al., 2009), which may benefit healing by providing starting materials more similar to those found naturally.

5 | CONCLUSION

Using an alternate soaking procedure, it is possible to use decellularized sheets of natively structured collagen fibrils to produce a scaffold of mineralized collagen reasonably matching the chemical makeup and structural organization seen in native bone, as determined using EDX, XRD, ATR-FTIR, SEM, and TEM. During the mineralization process, use of pAsp was confirmed to be important for close integration between collagen fibrils and the introduced mineral phase, as was citrate for limiting the plate size of crystals. The process described here may be a useful alternative approach for the development of bone regeneration scaffolds.

ACKNOWLEDGMENTS

This work was funded by a grant to SPV by the Natural Sciences and Engineering Research Council of Canada (NSERC). BHG thanks the Nova Scotia Health Research Foundation (NSHRF) for providing graduate stipend support. We acknowledge the support of the Canada Foundation for Innovation, the Atlantic Innovation Fund, and other partners which fund the Facilities for Materials Characterization, managed by the Clean Technologies Research Institute, Dalhousie University.

ORCID

Samuel P. Veres https://orcid.org/0000-0001-6308-4836

REFERENCES

Berg, J. K., Jordan, T., Binder, Y., & Gebauer, D. (2013). Mg2+ tunes the wettability of liquid precursors of CaCO3: Toward controlling mineralization sites in hybrid materials. *Journal of the American Chemical Society*, *135*, 12512–12515.

Berzina-Cimdina, L., & Borodajenko, N. (2012). Research of Calcium Phosphates Using Fourier Transform Infrared Spectroscopy. In Theophanides Theophile, (Ed.), *Infrared Spectroscopy - Materials Science, Engineering and Technology*. (pp. 123–148). London: InTech.

Calabrese, G., Giuffrida, R., Forte, S., Salvatorelli, L., Fabbi, C., Figallo, E., … Gulino, R. (2016). Bone augmentation after ectopic implantation of a cell-free collagen-hydroxyapatite scaffold in the mouse. *Nature Scientific Reports*, *6*, 36399.

Chatelain, G., Bourgeois, D., Ravaux, J., Averseng, O., Vidaud, C., & Meyer, D. (2013). Alternate dipping preparation of biomimetic apatite layers in the presence of carbonate ions. *Biomedical Materials*, *9*, 015003.

Cheng, X., Varona, P. L., Olszta, M. J., & Gower, L. B. (2007). Biomimetic synthesis of calcite films by a polymer-induced liquid-precursor (PILP) process: 1. Influence and incorporation of magnesium. *Journal of Crystal Growth*, *307*, 395–404.

Cölfen, H. (2007). Bio-inspired Mineralization Using Hydrophilic Polymers. In K. Naka, (Ed.), Biomineralization II. Topics in Current Chemistry, (vol. *271*, pp. 1–77). Berlin, Heidelberg: Springer-Verlag.

Delgado, L. M., Bayon, Y., Pandit, A., & Zeugolis, D. I. (2015). To cross-link or not to cross-link? Cross-linking associated foreign body response of collagen-based devices. *Tissue Engineering, Part B: Reviews*, *21*, 298–313.

Delgado-López, J. M., Bertolotti, F., Lyngsø, J., Pedersen, J. S., Cervellino, A., Masciocchi, N., & Guagliardi, A. (2017). The synergic role of collagen and citrate in stabilizing amorphous calcium phosphate precursors with platy morphology. *Acta Biomaterialia*, *49*, 555–562.

Driessens, F., Bermudez, O., & Fernandez, E. (1994). Effective formulations for the preparation of calcium phosphate bone cements. *Journal of Materials Science: Materials in Medicine*, *5*, 164–170.

Driessens, F. C., & Verbeeck, R. K. (1990). *Biominerals* (pp. 1–416). Florida: CRC Press.

Farzadi, A., Bakhshi, F., Solati-Hashjin, M., Asadi-Eydivand, M., & Osman, N. A. A. (2014). Magnesium incorporated hydroxyapatite: Synthesis and structural properties characterization. *Ceramics International*, *40*, 6021–6029.

Fountos, G., Tzaphlidou, M., Kounadi, E., & Glaros, D. (1999). In vivo measurement of radius calcium/phosphorus ratio by X-ray absorptiometry. *Applied Radiation and Isotopes*, *51*, 273–278.

Gelinsky, M., Welzel, P. B., Simon, P., Bernhardt, A., & König, U. (2008). Porous three-dimensional scaffolds made of mineralised collagen: Preparation and properties of a biomimetic nanocomposite material for tissue engineering of bone. *Chemical Engineering Journal*, *15*, 84–96.

Girija, E. K., Yokogawa, Y., & Nagata, F. (2004). Apatite formation on collagen fibrils in the presence of polyacrylic acid. *Journal of Materials Science. Materials in Medicine*, *15*, 593–599.

Goes, J. C., Figueiro, S. D., Oliveira, A. M., Macedo, A. A., Silva, C. C., Ricardo, N. M., & Sombra, A. S. (2007). Apatite coating on anionic and native collagen films by an alternate soaking process. *Acta Biomaterialia*, *3*, 773–778.

Gower, L. B. (2008). Biomimetic model systems for investigating the amorphous precursor pathway and its role in biomineralization. *Chemical Review*, *108*, 4551–4627.

Gower, L. B. (2015). Biomimetic mineralization of collagen. In C. Aparicio & M. Ginebra (Eds.), *Biomineralization and biomaterials: Fundamentals and applications* (pp. 187–232). Amsterdam: Elsevier.

Gower, L. B., & Odom, D. J. (2000). Deposition of calcium carbonate films by a polymer-induced liquid-precursor (PILP) process. *Journal of Crystal Growth*, *210*, 719–734.

Gu, L.-S., Kim, J., Kim, Y. K., Liu, Y., & Ling, J.-Q. (2010). A chemical phosphorylation-inspired design for type I collagen biomimetic remineralization. *Dental Materials*, *26*, 1077–1089.

Hu, Y.-Y., Rawal, A., & Schmidt-Rohr, K. (2010). Strongly bound citrate stabilizes the apatite nanocrystals in bone. *Proceedings of the National Academy of Sciences of the United States of America*, *107*, 22425–22429.

Iafisco, M., Ramírez-Rodríguez, G. B., Sakhno, Y., Tampieri, A., Martra, G., Gómez-Morales, J., & Delgado-López, J. M. (2015). The growth mechanism of apatite nanocrystals assisted by citrate: Relevance to bone biomineralization. *CrystEngComm*, *17*, 507–511.

Ida, T., Kaku, M., Kitami, M., Terajima, M., Rocabado, J. M. R., Akiba, Y., … Uoshima, K. (2018). Extracellular matrix with defective collagen cross-linking affects the differentiation of bone cells. *PLoS One*, *13*, e0204306.

Jee, S. S., Culver, L., Li, Y., Douglas, E. P., & Gower, L. B. (2010). Biomimetic mineralization of collagen via an enzyme-aided PILP process. *Journal of Crystal Growth*, *312*(8), 1249–1256 [Presented at the 17th American Conference on Crystal Growth and Epitaxy/the 14th U.S. Biennial Workshop on Organometallic Vapor Phase Epitaxy/the 6th International Workshop on Modeling in Crystal Growth.].

Kikuchi, M., Itoh, S., Ichinose, S., Shinomiya, K., & Tanaka, J. (2001). Self-organization mechanism in a bone-like hydroxyapatite/collagen nanocomposite synthesized in vitro and its biological reaction in vivo. *Biomaterials*, *22*, 1705–1711.

Kim, D., Lee, B., Thomopoulos, S., & Jun, Y.-S. (2018). The role of confined collagen geometry in decreasing nucleation energy barriers to intrafibrillar mineralization. *Nature Communications*, *9*, 962.

Landi, E., Logroscino, G., Proietti, L., Tampieri, A., Sandri, M., & Sprio, S. (2008). Biomimetic mg-substituted hydroxyapatite: From synthesis to in vivo behaviour. *Journal of Materials Science. Materials in Medicine*, *19*, 239–247.

Li, C.-P., Enomoto, H., Hayashi, Y., Zhao, H., & Aoki, T. (2010). Recent advances in phosphorylation of food proteins: A review. *LWT--Food Science and Technology*, *43*, 1295–1300.

Li, X., & Chang, J. (2008). Preparation of bone-like apatite–collagen nanocomposites by a biomimetic process with phosphorylated collagen. *Journal of Biomedical Materials Research*, *85A*, 293–300.

Liao, S., Watari, F., Uo, M., Ohkawa, S., Tamura, K., Wang, W., & Cui, F. (2005). The preparation and characteristics of a carbonated hydroxyapatite/collagen composite at room temperature. *Journal of Biomedical Materials Research. Part B, Applied Biomaterials*, *74*, 817–821.

Lickorish, D., Ramshaw, J. A., Werkmeister, J. A., Glattauer, V., & Howlett, C. R. (2004). Collagen–hydroxyapatite composite prepared by biomimetic process. *Journal of Biomedical Materials Research. Part B, Applied Biomaterials*, *68*, 19–27.

Lin, K.-F., He, S., Song, Y., Wang, C.-M., Gao, Y., Li, J.-Q., … Pei, G.-X. (2016). Low-temperature additive manufacturing of biomimic three-dimensional hydroxyapatite/collagen scaffolds for bone regeneration. *ACS Applied Materials & Interfaces*, *8*, 6905–6916.

Linhart, W., Peters, F., Lehmann, W., Schwarz, K., Schilling, A. F., Amling, M., … Epple, M. (2001). Biologically and chemically optimized composites of carbonated apatite and polyglycolide as bone substitution materials. *Journal of Biomedical Materials Research*, *54*, 162–171.

Liu, W., Yeh, Y.-C., Lipner, J., Xie, J., Sung, H.-W., Thomopoulos, S., & Xia, Y. (2011). Enhancing the stiffness of electrospun nanofiber scaffolds with a controlled surface coating and mineralization. *Langmuir*, *27*, 9088–9093.

Lyons, F. G., Gleeson, J. P., Partap, S., Coghlan, K., & O'Brien, F.J. (2014). Novel Microhydroxyapatite Particles in a Collagen Scaffold: A Bioactive Bone Void Filler? *Clin Orthop Relat Res*. *472*, 1318–1328.

Manjubala, I., & Sivakumar, M. (2001). In-situ synthesis of biphasic calcium phosphate ceramics using microwave irradiation. *Materials Chemistry and Physics*, *71*, 272–278.

Marzec, M., Kucińska-Lipka, J., Kalaszczyńska, I., & Janik, H. (2017). Development of polyurethanes for bone repair. *Materials Science and Engineering: C*, *80*, 736–747.

Matheis, G., & Whitaker, J. R. (1984). Chemical phosphorylation of food proteins: An overview and a prospectus. *Journal of Agricultural and Food Chemistry*, *32*, 699–705.

Meejoo, S., Maneeprakorn, W., & Winotai, P. (2006). Phase and thermal stability of nanocrystalline hydroxyapatite prepared via microwave heating. *Thermochimica Acta*, *447*, 115–120.

Moradian-Oldak, J., Weiner, S., Addadi, L., & Traub, W. (1991). Electron imaging and diffraction study of individual crystals of bone, mineralized tendon and synthetic carbonate apatite. *Connective Tissue Research*, *25*, 219–228.

Mousa, S., & Hanna, A. (2013). Synthesis of nano-crystalline hydroxyapatite and ammonium sulfate from phosphogypsum waste. *Materials Research Bulletin*, *48*, 823–828.

Nudelman, F., Pieterse, K., George, A., Bomans, P. H., Friedrich, H., Brylka, L. J., … Sommerdijk, N. A. (2010). The role of collagen in bone apatite formation in the presence of hydroxyapatite nucleation inhibitors. *Nature Materials*, *9*, 1004–1009.

Olszta, M. J., Cheng, X., Kumar, R., Kim, Y.-Y., Kaufman, M. J., & Douglas, E. P. (2007). Bone structure and formation: A new perspective. *Materials Science & Engineering R: Reports*, *58*, 77–116.

Olszta, M. J., Douglas, E. P., & Gower, L. B. (2003). Scanning electron microscopic analysis of the mineralization of type I collagen via a polymer-induced liquid-precursor (PILP) process. *Calcified Tissue International*, *72*, 583–591.

Partap, S., & Coghlan, K. (2014). Novel microhydroxyapatite particles in a collagen scaffold: A bioactive bone void filler. *Clinical Orthopaedics and Related Research*, *472*, 1318–1328.

Politi, Y., Batchelor, D. R., Zaslansky, P., Chmelka, B. F., Weaver, J. C., Sagi, I., … Addadi, L. (2009). Role of magnesium ion in the stabilization of biogenic amorphous calcium carbonate: A structure–function investigation. *Chemistry of Materials*, *22*, 161–166.

Posner, A. S., & Betts, F. (1975). Synthetic amorphous calcium phosphate and its relation to bone mineral structure. *Accounts of Chemical Research*, *8*, 273–281.

Pugely, A. J., Petersen, E. B., DeVries-Watson, N., & Fredericks, D. C. (2017). Influence of 45S5 bioactive glass in a standard calcium phosphate collagen bone graft substitute on the Posterolateral fusion of rabbit spine. *The Iowa Orthopaedic Journal*, *37*, 193–198.

Raynaud, S., Champion, E., Bernache-Assollant, D., & Thomas, P. (2002). Calcium phosphate apatites with variable Ca/P atomic ratio. I. Synthesis, characterisation and thermal stability of powders. *Biomaterials*, *23*, 1065–1072.

Rey, C., Combes, C., & Drouet, C. (2009). Bone mineral: Update on chemical composition and structure. *Osteoporosis International*, *20*, 1013–1021.

Schemitsch, E. H. (2017). Size matters: Defining critical in bone defect size. *Journal of Orthopaedic Trauma*, *31*, S20–S22.

Schmitz, J. P., & Hollinger, J. O. (1986). The critical size defect as an experimental model for craniomandibulofacial nonunions. *Clinical Orthopaedics and Related Research*, *205*, 299–308.

Shao, C., Zhao, R., Jiang, S., Yao, S., Wu, Z., Jin, B., … Tang, R. (2018). Citrate improves collagen mineralization via interface wetting: A physicochemical understanding of biomineralization control. *Advanced Materials*, *30*(8), 1704876.

Shen, C. Y. (1966). Alkaline hydrolysis of sodium Trimetaphosphate in concentrated solutions and its role in built detergents. *I&EC Product Research and Development*, *5*, 272–276.

Taguchi, T., Shiraogawa, M., Kishida, A., & Akashi, M. (1999). A study on hydroxyapatite formation on/in the hydroxyl groups-bearing nonionic hydrogels. *Journal of Biomaterials Science*, *10*, 19–32.

Talari, A. C. S., Martinez, M. A. G., Movasaghi, Z., Rehman, S., & Rehman, I. U. (2017). Advances in Fourier transform infrared (FTIR) spectroscopy of biological tissues. *Applied Spectroscopy Reviews*, *52*, 456–506.

Tampieri, A., Celotti, G., Landi, E., Sandri, M., Roveri, N., & Falini, G. (2003). Biologically inspired synthesis of bone-like composite: Self-assembled collagen fibers/hydroxyapatite nanocrystals. *Journal of Biomedical Materials Research. Part B, Applied Biomaterials*, *67*, 618–625.

Tomoaia, G., & Pasca, R.-D. (2015). On the collagen mineralization. A review. *Clujul Med*, *88*, 15–22.

Tzaphlidou, M., & Zaichick, V. (2004). Sex and age related Ca/P ratio in cortical bone of iliac crest of healthy humans. *Journal of Radioanalytical and Nuclear Chemistry*, *259*, 347–349.

Ulian, G., Valdrè, G., Corno, M., & Ugliengo, P. (2013). The vibrational features of hydroxylapatite and type a carbonated apatite: A first principle contribution. *American Mineralogist*, *98*, 752–759.

Villa, M. M., Wang, L., Huang, J., Rowe, D. W., & Wei, M. (2015). Bone tissue engineering with a collagen–hydroxyapatite scaffold and culture expanded bone marrow stromal cells. *Journal of Biomedical Materials Research. Part B, Applied Biomaterials*, *103*, 243–253.

Wang, Y., Hua, Y., Zhang, Q., Yang, J., Li, H., Li, Y., … Zhang, X. (2018). Using biomimetically mineralized collagen membranes with different surface stiffness to guide regeneration of bone defects. *Journal of Tissue Engineering and Regenerative Medicine*, *12*, 1545–1555.

Wasiak, J. (2015). Bone grafts and bone substitutes for opening-wedge osteotomies of the knee: A systematic review. *Arthroscopy*, *31*, 720–730.

Weisgerber, D. W., Caliari, S. R., & Harley, B. A. (2015). Mineralized collagen scaffolds induce hMSC osteogenesis and matrix remodeling. *Biomaterials Science*, *3*, 533–542.

Woods, T., & Gratzer, P. F. (2005). Effectiveness of three extraction techniques in the development of a decellularized bone–anterior cruciate ligament–bone graft. *Biomaterials*, *26*, 7339–7349.

Xie, B., & Nancollas, G. H. (2010). How to control the size and morphology of apatite nanocrystals in bone. *Proceedings of the National Academy of Sciences of the United States of America*, *107*, 22369–22370.

Yokoyama, A., Gelinsky, M., Kawasaki, T., Kohgo, T., König, U., Pompe, W., & Watari, F. (2005). Biomimetic porous scaffolds with high elasticity made from mineralized collagen—An animal study. *Journal of Biomedical Materials Research. Part B, Applied Biomaterials*, *75*, 464–472.

Zhang, D., Wu, X., Chen, J., & Lin, K. (2018). The development of collagen based composite scaffolds for bone regeneration. *Bioactive Materials*, *3*, 129–138.

Zheng, H., Bai, Y., Hoffmann, C., Peters, F., & Waldner, C. (2014). Effect of a β-TCP collagen composite bone substitute on healing of drilled bone voids in the distal femoral condyle of rabbits. *Journal of Biomedical Materials Research. Part B, Applied Biomaterials*, *102*, 376–383.

How to cite this article: Grue BH, Veres SP. Use of tendon to produce decellularized sheets of mineralized collagen fibrils for bone tissue repair and regeneration. *J Biomed Mater Res*. 2020; 108B:845–856. https://doi.org/10.1002/jbm.b.34438